Decoherence-protected spin-photon quantum gates in a hybrid semiconductor-superconductor circuit

Li Wang, Tao Tu,* Bo Gong, and Guang-Can Guo
Key Laboratory of Quantum Information, University of Science and Technology of China, Chinese Academy of Sciences, Hefei 230026, People's Republic of China

(Received 29 October 2015; revised manuscript received 9 November 2015; published 30 December 2015)

High-fidelity gate operations are a crucial function for quantum information processing. This problem is particularly challenging for hybrid systems where coherence and control time scales greatly differ by orders of magnitude among different elements. Here we propose decoherence-protected gate operations in an important class of hybrid system in the context of a spin qubit in semiconductor quantum dots coupled to a superconductor resonator. Our scheme is able to generate complex photon states for various applications even in the presence of practical imperfections: limited available control of the spin-photon hybrid system and demanding spin decoherence in current state-of-the-art devices.

DOI: 10.1103/PhysRevA.92.062346 PACS number(s): 03.67.Lx, 42.50.Dv, 42.50.Pq, 85.25.−j

I. INTRODUCTION

Cavity quantum electrodynamics (CQED) is a promising hybrid system, in which the production of quantum optical states is crucial for valuable resources of quantum information processing [1–4]. For solid-state circuits, nonclassical states of superconducting resonators have played important roles for several uses: coherently transferring quantum information between two spatially separated qubits is implemented with the resonator field [5], a quantum nondemolition measurement of a qubit is realized by resonator probes [6,7], a generator of single microwave photons is achieved by controllable interactions between resonators and qubits [8,9], and a quantum memory to store and shuttle information can be built with a resonator due to its large Hilbert space [10–13]. There have been some schemes for the creation of complex photon states in superconducting resonators; however, most methods developed thus far are based on manipulating photons and qubits step by step [14,15]. These implementations become increasingly burdensome and difficult to realize because of the long operation time that is necessary within the short decoherence time.

Electron spins in semiconductor quantum dots are among the leading candidates for a qubit [16]. Recently, a CQED architecture has been employed to couple electron spins trapped in a semiconductor double quantum dot with photons stored in a superconducting resonator [17–24]. As the CQED methods hold promise for uses in the context of quantum technologies, it is timely to establish a set of efficient spin-photon gate operations. A quantum system is unavoidably affected by couplings to the environment, preventing high-fidelity performance for any quantum information task. Dynamical decoupling, an approach that applies fast qubit flips to average out the interactions with the outside world, is a practical and powerful tool for coherence protection [25]. An individual qubit can be efficiently protected by dynamical decoupling [26–33]; however, combining the decoupling technique with hybrid systems is obviously problematic. In general, the decoupling does not distinguish the interactions of different elements from the coupling to the environment, and it eliminates both. Hence, the decoupling disrupts the dynamics of different elements and conflicts with interelement operations [34–36]. For a CQED system consisting of electron spins and photons, this problem is particularly salient where coherence and control time scales greatly differ by orders of magnitude among the electron spins in quantum dots and the photons in a superconducting resonator. As a result, decoherence-protected quantum operations in CQED systems have thus far remained elusive and are highly desirable.

Here we propose a decoherence-protected spin-photon gate that allows the integration of decoupling into operations for CQED hybrid architectures. The key idea is to design the evolution intervals between the electron-spin decoupling to meet the photon dynamics. This design preserves all of the advantages of dynamical decoupling without requiring both spin and photons to be controlled on similar time scales or requiring the decoupling control to commute with the spin-photon interaction. When working in the dispersive regime, this yields a spin-state conditional phase shift of photons, and at the same time the electron-spin qubit is dynamically protected. Unlike previous schemes, we can create a set of spin-photon operations, providing an efficient and self-protected method to manipulate coherent states of photons with arbitrary phase and amplitude, for example, generating entangled states of spin and photons, deterministically encoding information from the spin state into the photon state, and creating multicomponent photon states. This decoherence-protected spin-photon gate could enable a variety of powerful methods for using resonator states in quantum information tasks, and it can be readily applied to a range of hybrid systems.

II. CQED WITH SPIN AND PHOTON

Usually, the weak magnetic dipole of a single electron spin makes it difficult to couple directly with a photon in the resonator. An alternative approach to spin-photon coupling relies on the spin-charge conversion, which mixes spin and charge degrees of freedom, resulting in spin states that have some charge character. Because the interaction between the charge dipole of electrons and the electric field of the resonator

*tutao@ustc.edu.cn

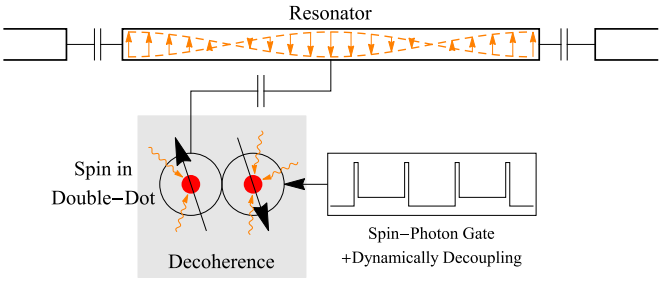

FIG. 1. (Color online) Schematic of the electron-spin qubit in double dot coupled to photons in a transmission line resonator. The goal is to design dynamical decoupling for a spin qubit, thus ensuring that the spin-photon gates are protected against decoherence instead of being disrupted by it.

is strong, this enables an effective spin-photon coupling rate of MHz [17], which is useful for many quantum information tasks.

We consider the specific CQED architecture to interface electron spins with a superconducting resonator outlined in Fig. 1. Here the double quantum dot forms a simple double-well confinement potential to hold two electrons. The potential difference ϵ between the two dots changes the charge configuration (n_L,n_R), where the notation n_L, n_R labels the number of electrons in the left and right quantum dot, respectively. The logical basis of our qubit is defined by the spin singlet and triplet states: $|(1,1)S\rangle = (|\uparrow\downarrow\rangle - |\downarrow\uparrow\rangle)/\sqrt{2}$ and $|(1,1)T_0\rangle = (|\uparrow\downarrow\rangle + |\downarrow\uparrow\rangle)/\sqrt{2}$. Typically, a modest external magnetic field (100 mT) is applied to split the spin aligned states, $|(1,1)T_+\rangle = |\uparrow\uparrow\rangle$ and $|(1,1)T_-\rangle = |\downarrow\downarrow\rangle$. Initial-state preparation, measurement, a one-qubit universal gate, and a first two-qubit gate have been demonstrated experimentally for this single-triplet qubit in GaAs quantum dots [37–39]. In addition to the qubit states, an auxiliary singlet state with two electrons in one quantum dot, $|(0,2)S\rangle$, is coupled to the separated singlet, $|(1,1)S\rangle$, via tunneling t. We model this double dot as a three-level system with the Hamiltonian

$$H_D = \epsilon|(0,2)S\rangle\langle(0,2)S| + t|(1,1)S\rangle\langle(0,2)S| + h|(1,1)S\rangle\langle(1,1)T_0| + \text{H.c.} \quad (1)$$

Here, $h = g\mu_B\Delta B$, ΔB is a static magnetic-field gradient between the two dots, which could be produced by dynamical nuclear spin polarizations or nearby permanent magnets [38].

We consider a superconducting transmission line resonator of length L, with capacitance per unit length C_0, and impedance Z_0. Neglecting the higher-energy modes, we can focus on the full wave mode of the resonator, with the wave vector $k = \frac{\pi}{L}$ and frequency $\omega = \frac{k}{C_0 Z_0}$ [40]. We quantize the electric field of the resonator as $\hat{V} = \sqrt{\frac{\hbar\omega}{LC_0}}(a + a^\dagger)$, and the resonator can be described by the Hamiltonian $H_R = \hbar\omega a^\dagger a$, where $a^\dagger$ and a are the creation and annihilation operator of the lowest-energy mode, respectively.

The interaction between the electrons and resonator is included naturally by writing the bias ϵ as a contribution from static electric fields ϵ_0, and a contribution from the electric field $\hat{V}$ of the resonator: $\epsilon = \epsilon_0 + e\hat{V}\frac{C_c}{C_t}$. Here, C_c is the capacitive coupling of the resonator to the dot, while C_t is the total capacitance of the double dot. The interaction between the double dot and the resonator can be given by the Hamiltonian

$$H_I = g(a + a^\dagger)|(0,2)S\rangle\langle(0,2)S|, \quad (2)$$

where $|(0,2)S\rangle\langle(0,2)S|$ represents the charge dipole and the coefficient $g = e\frac{C_c}{C_t LC_0}\sqrt{\frac{\hbar\pi}{Z_0}}$ is the vacuum Rabi coupling. By changing the bias parameter to be near the (1,1) to (0,2) singlet transition, we can obtain the electron-spin eigenstates of the double dot: $|\Uparrow\rangle = \cos\eta|\uparrow\downarrow\rangle + \sin\eta|(0,2)S\rangle$, $|\Downarrow\rangle = -\sin\eta|\uparrow\downarrow\rangle + \cos\eta\ |(0,2)S\rangle$ using degenerate perturbation theory in the tunneling t [41,42]. Here, the energy gap between $|\uparrow\downarrow\rangle$ and $|(0,2)S\rangle$ is $\omega_a = \sqrt{(h-\epsilon_0)^2 + 4t^2}$ and the mixing angle is $\eta = \frac{1}{2}\arctan(\frac{2t}{h-\epsilon_0})$. Putting things together, in the rotating frame, we obtain a combined Hamiltonian of the hybrid system

$$H_t = \hbar\Delta|\Downarrow\rangle\langle\Downarrow| + g_{\text{eff}}a|\Downarrow\rangle\langle\Uparrow| + \text{H.c.}, \quad (3)$$

where $\Delta = \omega_a - \omega_0$ is the qubit detuning from the resonator, and the coupling strength is $g_{\text{eff}} = -\frac{1}{2}g\sin 2\eta$.

III. SPIN-STATE CONDITIONAL OPERATION OF PHOTONS

In previous schemes for the CQED system, one can control the qubit-resonator interaction by adjusting the qubit frequency on resonance ($\Delta = 0$). On resonance, the coupling will produce an oscillation between the qubit and resonator, say, $|n\rangle \otimes |\Uparrow\rangle$, the qubit in its ground state with n photons in the resonator, and $|n-1\rangle \otimes |\Downarrow\rangle$, the qubit in its excited state with $n-1$ photons in the resonator. This operation between qubit and photon can be implemented to synthesize arbitrary states in the resonator [14,15]. However, for an unprotected operation, of duration τ, the gate fidelity is limited by the electron-spin dephasing, which is dominated either by charge noise [43] or nuclear spin fluctuations [44]. Dynamical decoupling applied to the electron spin suppresses decoherence while also disrupting the spin-photon coupling. Moreover, because a photon in the resonator has a longer decay time (typically $> 10\ \mu$s) than the electron spin's dephasing time (approximately 10 ns for a GaAs quantum dot system), a synchronized application of the dynamical decoupling to both the spin and photon is obviously problematic.

In our design, we realize the spin-photon quantum operation by using a dispersive coupling of the double dot and the resonator [45]. When the quantum dot is detuned from the resonator by Δ, the effective Hamiltonian in the off-resonant regime can be described as

$$H_{\text{eff}} = \hbar\Delta|\Downarrow\rangle\langle\Downarrow| - \kappa a^\dagger a|\Downarrow\rangle\langle\Downarrow|, \quad (4)$$

where κ is the dispersive interaction between the spin state of the double dot and photon mode of the resonator. When the system is under free evolution of the dispersive Hamiltonian for a time τ_n, the conditional resonator phase shift operator can be produced as

$$U_{\phi_n} = I \otimes |\Uparrow\rangle\langle\Uparrow| + e^{i\phi_n a^\dagger a} \otimes |\Downarrow\rangle\langle\Downarrow|, \quad (5)$$

where $\phi_n = \kappa\tau_n$ is the phase shift induced on the resonator state and I is the identity operator.

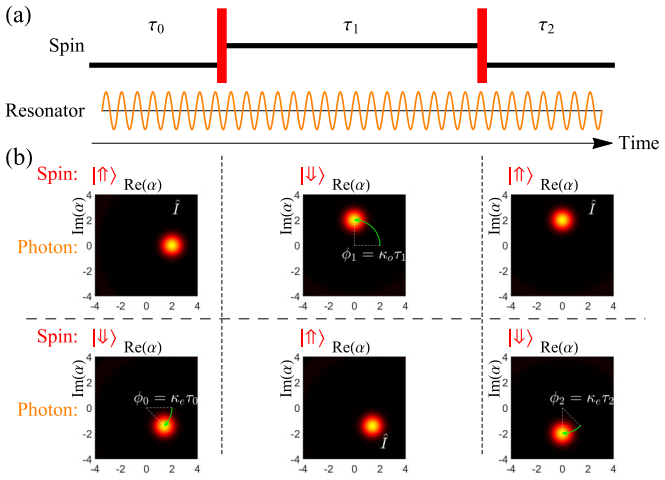

FIG. 2. (Color online) (a) The designed decoherence-protected spin-photon gate, consisting of the dynamical decoupling of the electron spin and dispersive coupling between the spin and photon. Here the number of decoupling pulses $N = 2$. (b) Snapshots of the corresponding spin-photon hybrid states at different stages of the operation. The Wigner function diagram shows the photon dynamics, conditioned on the initial spin state, during the gate operation.

In parallel with driving the resonator, we decouple the electron spin from the environment using short electric pulses that constantly switch the electron spin between states $|\Uparrow\rangle$ and $|\Downarrow\rangle$ [Fig. 2(a)]. The decoupling sequence consists of repeating the basic unit $\tau_{n-1} - X_\pi - \tau_n$, where X_π is the decoupling pulse that flips the electron-spin states around the x axis on the Bloch sphere and τ_n is the interpulse delay. At first, such a conditional operation seems to contradict the decoupling sequence. However, it can be fulfilled in a designed situation where the interpulse evolution matches the spin and photon coupling such that the decoupling pulses are applied in resonance with the dynamics of the photon in the resonator. This design provides an approach for selective coupling of the fast spin qubit to the slow photon states while decoupling all others.

For an N-pulse dynamical decoupling sequence, it is achieved by adjusting the qubit detuning between two operating points, one with dispersive coupling κ_e for the even nth interval, and the other with κ_o for odd n. Thus, the photon acquires a phase shift by ϕ_n during the interval τ_n if the electron is in the state $|\Downarrow\rangle$. If the electron is in the state $|\Uparrow\rangle$ during the time interval τ_n, however, the photon does nothing. The overall dynamics are shown in Fig. 2(b); the photon attains a different phase shift depending on the initial state of the electron, where we use realistic parameters $\kappa_e/2\pi = -\kappa_o/2\pi = 1.3$ MHz, $\tau_1 = 2\tau_0 = 2\tau_2 = 2\tau = 96$ ns in experiments [17,29]. An unconditional phase shift of the photon, independent of the electron-spin state, is constructed from the same operation by choosing $\kappa_e = \kappa_o$ (see appendixes for details). From the conditional and unconditional operations, we can implement a full set of gates for the spin-photon hybrid system.

We implement the controlled phase gate and the Wigner tomography data in Fig. 2(b) to confirm the selectivity of this gate. To consider the effect of decoherence in a gate operation, we introduce two sources of noise invariably present in a singlet-triplet qubit system: spin noise and charge noise (see appendixes for details of the theoretical modeling and simulation). To characterize the gate fully, we use the Wigner function $W(\alpha)$ of its action, which is a representation of a photon state in the resonator phase space. For a coherent state $|\alpha\rangle$ of the resonator, the photon rotates in an anticlockwise direction by the angle $\phi = 2\kappa_e\tau$ if the electron spin is initially in state $|\Downarrow\rangle$ or in a clockwise direction if the electron spin is initially in state $|\Uparrow\rangle$.

IV. DECOHERENCE-PROTECTED GENERATION OF VARIOUS PHOTON STATES

We exploit this conditional shift operation to implement spin-photon entanglement. For example, we start with an unentangled spin-photon state $|\alpha\rangle \otimes (|\Uparrow\rangle + |\Downarrow\rangle)$, applying a conditional phase shift operation on the initial state, which produces an entangled spin-photon state $|\alpha e^{-i\phi}\rangle \otimes |\Uparrow\rangle + |\alpha e^{i\phi}\rangle \otimes |\Downarrow\rangle$. When the total phase ϕ equals $\frac{\pi}{2}$, this state corresponds to a Schrödinger cat, where the spin state is entangled with the phases of the superimposed coherent states. This state has been studied in other quantum systems, while in this case the preparation is deterministic, unlike methods involving probabilistic projective measurements. By using this method, we create and confirm a typical cat state as shown in Fig. 3(a). In addition, this protocol can directly scale to resonator states with larger amplitude, which has potential in phase sensitivity measurement.

This procedure can be generalized to any arbitrary spin state $\cos\frac{\theta}{2}|\Uparrow\rangle + \sin\frac{\theta}{2}|\Downarrow\rangle$, that maps as $\cos\frac{\theta}{2}|\alpha e^{-i\phi}\rangle \otimes |\Uparrow\rangle + \sin\frac{\theta}{2}|\alpha e^{i\phi}\rangle \otimes |\Downarrow\rangle$. Here, θ is the parameter of the initial spin state. Using this tool, one can deterministically encode quantum information in a cat state by creating a desired superposition of coherent states conditioned on an initial spin state. Figure 3(b) shows the creation of cat states conditioned by spin prepared at initial state $\theta = \frac{\pi}{3}$. Two special forms of cat states, known as the even or odd cat states $|\alpha\rangle \otimes |\Downarrow\rangle + |-\alpha\rangle \otimes |\Uparrow\rangle$, $|\alpha\rangle \otimes |\Downarrow\rangle - |-\alpha\rangle \otimes |\Uparrow\rangle$, can be obtained by setting $\phi = \frac{\pi}{2}$ and $\theta = \pi$, $-\pi$, respectively. Because a coherent state is a superposition of Fock states, these states produce superpositions of only even or odd photon numbers, which can be used to measure the resonator photon parity.

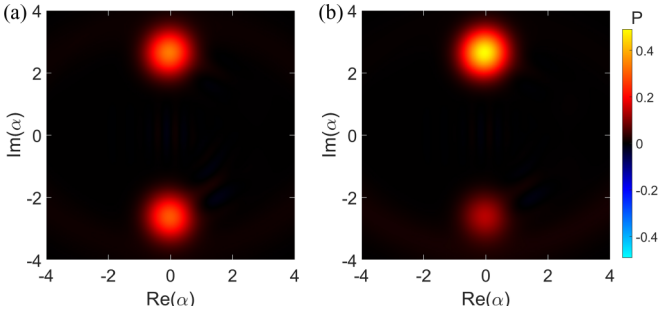

FIG. 3. (Color online) (a) Wigner function of the generated photon coherent-state superposition $|\alpha e^{-i\phi}\rangle + |\alpha e^{i\phi}\rangle$. (b) One can encode information in a photon state by creating an arbitrary superposition of coherent states $\cos\frac{\theta}{2}|\alpha e^{-i\phi}\rangle + \sin\frac{\theta}{2}|\alpha e^{i\phi}\rangle$ conditioned on an initial qubit state. Here $\alpha = \sqrt{7}$, $\phi = \frac{\pi}{2}$ in (a) and (b).

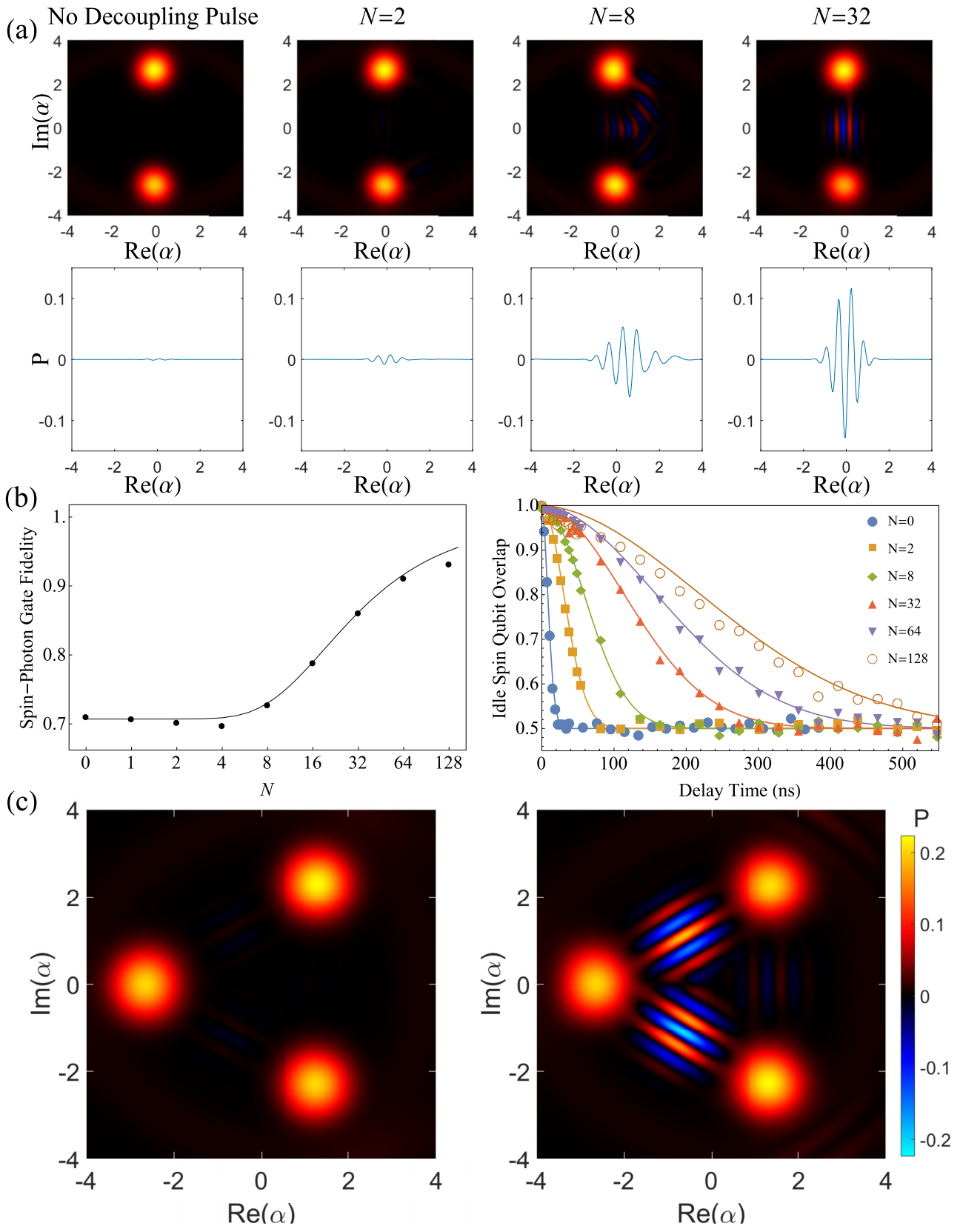

FIG. 4. (Color online) (a) The Wigner function (top) and cut along the imaginary axis (bottom) of the created photon states for an increasing number of decoupling pulses, N. (b) Left: Fidelity of the gate operation shown in (a), as a function of the number of decoupling pulses. Right: For comparison, the coherence time of the idle electron-spin qubit, not involved in the gate operation, is also effectively prolonged by applying the same decoupling pulses. (c) Multicomponent photon states executed with (right) and without (left) the decoherence-protected spin-photon gate.

A crucial step in this work is confirming that our design ensures efficient protection during the gate operation in the presence of strong decoherence. We first study the fidelity of the conditional phase $\phi = \frac{\pi}{2}$ shift gate as a function of the number of decoupling pulses applied during its gate time. The operation requirements are maintained as the number of pulses is increased. We apply the gate to the initial state $|\Psi_i\rangle = |\alpha\rangle \otimes (|\Downarrow\rangle + |\Uparrow\rangle)$; this ideally yields the entangled state $|\Psi_f\rangle = |\alpha\rangle \otimes |\Downarrow\rangle + |-\alpha\rangle \otimes |\Uparrow\rangle$ (neglecting an i factor). Cuts along the real and imaginary axes of the Wigner function reveal the relative population and quantum interference of the superimposed coherent states. As shown in Fig. 4(a), the quantum state tomography of the hybrid system reveals that the coherence of the final state, displayed by the imaginary parts of the Wigner function, grows with the number of pulses.

The state fidelity [Fig. 4(b)], $F = \sqrt{\langle\Psi_f|\rho|\Psi_f\rangle}$, reaches 93% when there are 64 decoupling pulses; this indicates the high performance of the gate operation, which is similar to the ideal scenario in which no decoherence is introduced. We notice that the gate efficiency remains high even in the regime where the gate time exceeds the dephasing time of the qubit. Then, we verify that the decoherence can be efficiently suppressed at the single-qubit level by the same dynamical decoupling. As shown in Fig. 4(b), we find that the electron-spin coherence time increases as the number of the decoupling pulses is increased. The comparison between the two figures in Fig. 4(b) demonstrates that the electron-spin coherence during the course of the conditional gate operation is preserved as efficiently as it is for an idle electron-spin qubit. More simulations provide evidence that the fidelity of the conditional gate remains high even in the presence of much stronger decoherence noise (see appendixes for details). Although a conventional N-pulse dynamical decoupling sequence is enough for decoherence protection, the present design is convenient for further optimization by using advanced sequences [46–50] (see appendixes for details).

Finally we illustrate the power of the decoherence-protected gates by the generation of more complicated states in this hybrid system. Unlike building photon states one by one, this method can be easily implemented to create more complex nonclassical resonator states. By using a conditional resonator phase shift for various phases ϕ, we can encode quantum information in a particular phase and then create superpositions of multiple coherent states. For example, we concatenate gates for $\phi = \frac{2\pi}{3}$ and $\frac{\pi}{3}$ to create three-component coherent states, and scaling to four-component states and more is straightforward (see appendixes for the circuit diagram of the multicomponent state preparation sequences). The diagram of the photon state tomography is given in Fig. 4(c), for the target state. Because the total execution time is almost 100 times longer than the electron-spin dephasing time, the complete implementing of the task is impossible without decoherence protection. However, the fidelity of the resulting state is still as high as 91%.

V. CONCLUSION

In summary, we propose a scheme of decoherence-protected quantum gates in a hybrid spin-photon system based on well-designed decoupling pulses applied to a spin qubit. This method opens the way to high-fidelity preparation of complex photon states, which are critical tasks for future quantum information processing. Moreover, this gate design marks an important step toward high-fidelity transfer, processing, and retrieval of quantum information in a hybrid architecture.

ACKNOWLEDGMENTS

This work was funded by the National Fundamental Research Program and the National Natural Science Foundation of China (Grants No. 11274294 and No. 11474270).

APPENDIX A: UNCONDITIONAL SPIN-PHOTON GATE OPERATION

In the present paper we design the gate with integrated decoupling for the spin-photon hybrid system. The dynamics of the system subjected to the dispersive coupling and the decoupling pulses are determined by the evolution operator over the gate units [the gate unit is depicted in Fig. 2(a) of the main text]. Each decoupling pulse interchanges the electron-spin qubit states between $|\Uparrow\rangle$ and $|\Downarrow\rangle$, so the total evolution operator per gate unit is

$$\begin{aligned} U &= U_{\Uparrow} \otimes |\Uparrow\rangle\langle\Uparrow| + U_{\Downarrow} \otimes |\Downarrow\rangle\langle\Downarrow|, \\ U_{\Uparrow} &= I \exp(i\phi_1 a^\dagger a) I, \\ U_{\Downarrow} &= \exp(i\phi_0 a^\dagger a) I \exp(i\phi_2 a^\dagger a), \end{aligned} \tag{A1}$$

where I is the identity operator and $\phi_0 = \kappa_e \tau_0$, $\phi_1 = \kappa_o \tau_1$, $\phi_2 = \kappa_e \tau_2$ are the phases accumulated in the unit τ_0, τ_1, τ_2, respectively.

To be specific, we explicitly calculate the conditional phase operator for a conventional $N = 2$ dynamical decoupling pulse, $\kappa_e = -\kappa_0$, $\tau_0 = \tau_2 = \tau$, and $\tau_1 = 2\tau$:

$$U = \exp(-i\phi a^\dagger a) \otimes |\Uparrow\rangle\langle\Uparrow| + \exp(i\phi a^\dagger a) \otimes |\Downarrow\rangle\langle\Downarrow|, \tag{A2}$$

i.e., the photon evolution over the units is a phase rotation by the angle $\phi = 2\kappa_e \tau$ in the anticlockwise or clockwise direction conditioned on the state of the electron-spin qubit. The Wigner function representation of this condition evolution is given in Fig. 2(b) of the main text.

This consideration also shows how to perform an unconditional phase operation of the photon in the resonator. In this case, we choose $\kappa_e = \kappa_0$, which is trivially achieved when adjusting the qubit frequency at the same operating points. In this case,

$$U = \exp(i\phi a^\dagger a) \otimes |\Uparrow\rangle\langle\Uparrow| + \exp(i\phi a^\dagger a) \otimes |\Downarrow\rangle\langle\Downarrow|, \tag{A3}$$

i.e., the phase shift is unconditional or does not depend on the electron-spin qubit input state. The Wigner function representation of the evolution of the photon during the unconditional phase shift gate is shown in Fig. 5.

Applying the conditional and unconditional gate sequentially, we can implement a full set of gates for the spin-photon hybrid system. It is also important to note that the Hamiltonian and operator are very general; thus, exploiting such a scheme could be a promising strategy for combining the quantum operation and dynamical decoupling to achieve decoherence-protected gates for a wide range of relevant hybrid systems.

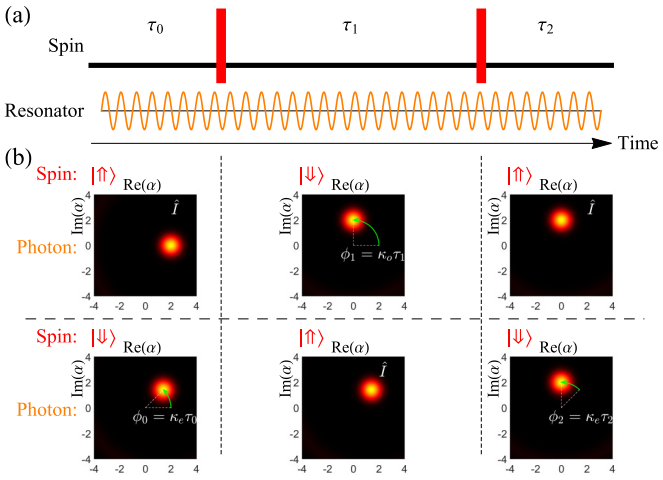

FIG. 5. (Color online) System dynamics during an unconditional phase shift with integrated decoupling, as visualized on the Wigner tomography. A gate contains two electron-spin qubit decoupling pulses and dispersive spin-photon coupling. By tuning $\kappa_e = \kappa_0$ such that $\phi = 2\kappa_e\tau$, the photon phase is rotated in the same direction for both electron-spin qubit states.

APPENDIX B: DECOHERENCE EFFECTS AND MASTER EQUATION OF THE HYBRID SYSTEM

The spin-photon gate operation discussed in the main text is a unitary and coherent process. However, in any experimental implementation, the undesired and unavoidable coupling to external degrees of freedom leads to decoherence, and thus it affects the observed dynamics behavior. To construct a realistic model for our system, we now discuss the decoherence problem in this spin-photon hybrid system.

The dissipation of the transmission line resonator occurs mainly through coupling to the external leads. In general the magnitude of this process can be described by the decay rate $\chi = \omega/Q$, where Q is the quality factor of the resonator [54,55]. In the reported high-finesse superconducting transmission line resonator with $Q = 1 \times 10^5$, the decay rate χ is of the order 0.1 MHz [4,17]. The influence of the photon decay is rather small compared to the electron-spin qubit even when the quality factor is lower, which greatly simplifies the implementation.

Precise manipulation of a singlet-triplet qubit is hindered by two sources of noise invariably present in GaAs quantum dot systems: One is fluctuations in the background nuclear spin bath due to hyperfine interaction, usually denoted as Overhauser noise or spin noise [44,51,52]; the other is fluctuations in the electrostatic confinement potential due to background charge impurities, usually denoted as charge noise [53]. The model Hamiltonian for our double-dot system is written in terms of

$$H_D = \epsilon|(0,2)S\rangle\langle(0,2)S| + t|(1,1)S\rangle\langle(0,2)S| + h|(1,1)S\rangle\langle(1,1)T_0| + \text{H.c.}, \tag{A4}$$

where $h = g\mu_B\Delta B$ is the energy associated with the magnetic-field gradient across the double dot, t is the tunneling coupling, and ϵ is the charge energy difference between separated and nonseparated singlet states, which can be controlled dynamically. Because both spin and charge noise are typically several orders of magnitude slower than spin gate times (approximately 1 nS), the resulting perturbations around h and ϵ are treated as random constants δh and $\delta\epsilon$, respectively.

The time evolution of the hybrid system is given by solving the time-dependent master equations of the density matrix as follows [56–58]:

$$\frac{d\rho}{dt} = -i[H_t,\rho] + D[L]\rho, \tag{A5}$$

where H_t is the total Hamiltonian of the hybrid system.

On one hand, L is the Liouvillian and D is the superoperators defined by $D[L]\rho = L^\dagger\rho L - \frac{1}{2}(L^\dagger L\rho - \rho L^\dagger L)$, and L are jump operators describing the environment process on the resonator, corresponding to the photon relaxation and dephasing. The jump operators corresponding to energy relaxation are defined by $L = \sqrt{2\chi}a$. For simulations reported here, the photon dephasing rate has been set to zero because the dominant effect of the environment is energy relaxation.

On the other hand, for the spin qubit Hamiltonian under investigation, incoherent effects are introduced by low-frequency fluctuations in the magnetic field δh and bias $\delta\epsilon$ with a Gaussian distribution. The offset δh from a stabilized h varies slowly with a measured deviation $\sigma_h = g\mu_B\sigma_{\Delta B}$ ($\sigma_{\Delta B} \approx 0.5$ mT [44,59]). For low-frequency charge noise, we use recent measurements of the standard deviation given as $\sigma_\epsilon \approx 8$ μeV [43].

In practice, we can simulate the evolution of the system by numerically solving Eq. (A5), using the dissipation rate parameter for the photon and averaged over many realizations of the spin and charge noise for the qubit. Each run has a stochastic term δh and $\delta\epsilon$, which is sampled from a Gaussian distribution of the noise with widths σ_h and σ_ϵ. The simulation results are shown in Figs. 2–4 in the main text. Similar numerical analysis has been used in a variety of quantum dot and circuit quantum electrodynamic settings [30,60,61].

APPENDIX C: FIDELITY OF THE SPIN-PHOTON GATE OPERATIONS

It is beneficial to quantify the performance of the spin-photon operations and evaluate the impact of noise effects. Thus, we can estimate the fidelity of each gate operation. We can adopt a gate fidelity defined as follows [57]:

$$F = \overline{|\langle\Psi(0)|U_P^+U_I|\Psi(0)\rangle|^2}, \tag{A6}$$

where U_I is the ideal unitary transformation matrix of the gate operation and U_P is the complex conjugate of the physical unitary transformation matrix. The definition can be naturally expressed as follows:

$$F = \text{Tr}[\rho_P(t)\rho_I(t)], \tag{A7}$$

where $\rho_P(t)$ and $\rho_I(t)$ are the physical and ideal density matrices, respectively, after the gate operation and Tr represents the trace. The $\rho_I(t)$ can be calculated using the unitary and coherent spin-photon operator discussed in the main text, and the $\rho_P(t)$ can be obtained as outlined in the above section.

In practice the charge noise has a significant effect for manipulation of a spin qubit in semiconductor quantum dots, especially for the materials such as silicon in which the nuclear

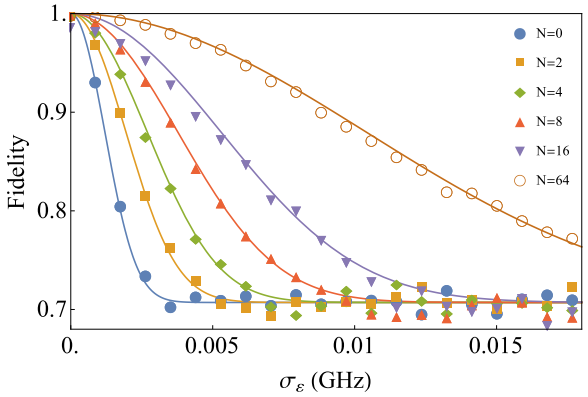

FIG. 6. (Color online) Gate fidelity vs charge noise with a Gaussian distribution of width σ_ϵ for different number N of decoupling pulses.

spin fluctuations are suppressed [48–50,62]. In Fig. 6 we show the spin-photon gate (conditional photon phase $\phi = \frac{\pi}{2}$ shift gate) fidelity as a function of charge noise fluctuations for different numbers of decoupling pulses. The results provide evidence that the fidelity of the conditional gate remains high even in the presence of much stronger decoherence noise.

APPENDIX D: NUMERICAL OPTIMIZATION OF THE GATE OPERATIONS

We have presented the designed spin-photon gates using the simple dynamical decoupling sequences discussed in Fig. 2 of the main text. These results reveal that by using more advanced optimization methods to extend the decoherence time a fidelity higher than 99% can be expected.

A conventional N-pulse dynamical decoupling sequence is characterized by just one timing parameter, namely, the pulse interval time. However, a general N-pulse sequence can be described as N timing parameters $\{\tau_n\}$ that comply with a set of dynamical decoupling constraints. The first-order criterion requires $\tau_0 - \tau_1 + \tau_2 + \cdots + (-1)^N \tau_N = 0$, the second-order criterion is a symmetric condition $\tau_n = \tau_{N-n}$, and higher-order criteria can be introduced straightforwardly. The optimization procedure can be summarized as the maximization of gate fidelity $F(\{\tau_n\})$ with respect to an N-pulse sequence $\{\tau_n\}$.

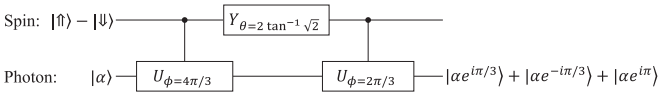

FIG. 7. The protocol for generating three-component coherent states. Here Y_θ is the rotation of electron spin by angle θ around the y axis on the Bloch sphere, and U_ϕ is the condition phase ϕ shift of photon states.

We adopt a numerical maximization protocol based on a scheme similar to the one described in the GRAPE algorithm [63]. Starting with initial timing parameters of $\{\tau_n\}_0$, in each maximization step, we update τ_n as $\tau_n + \delta\tau_n$, where $\delta\tau_n = \frac{\partial F}{\partial \tau_n}$ such that $\delta F \geqslant 0$. δF can be calculated through the straightforward evaluation of the density matrix in the master equation, which is discussed in Sec. II. The dynamical decoupling sequence $\{\tau_n\}$ is then found by the numerical optimization of F in the large parameter space. In general, it is nontrivial because of the nonlinearity and the large number of variables in the problem.

APPENDIX E: PREPARATION OF COMPLEX PHOTON STATES USING SPIN-PHOTON GATE OPERATIONS

As described in the main text, we have created a set of decoherence-protected spin-photon gate operations, allowing for control over the large resonator phase space with high fidelity. We can implement these operations to efficiently generate various superposition states, deterministically encoding information in a cat state by creating an arbitrary superposition of photon coherent states conditioned on an initial qubit state. Furthermore, we can concatenate these operations to encode information into multiple phases of the photon state, thereby creating multicomponent states. Figure 7 outlines the sequence of operations required to produce the example photon states shown in Fig. 4(c) of the main text. The phase shift of the conditional spin-photon gate will determine the phase of each coherent state.

The set of operations demonstrated here provides an efficient and high-fidelity method to manipulate photon states and could enable a variety of powerful methods for using photon states in quantum information tasks. For example, it can also be used on a spin qubit coupled to two spatially separated resonators to prepare nonlocal mesoscopic superposition states of the resonator.

[1] Z. L. Xiang, S. Ashhab, J. Q. You, and F. Nori, Rev. Mod. Phys. **85**, 623 (2013).
[2] J. M. Raimond, T. Meunier, P. Bertet, S. Gleyzes, P. Maioli, A. Auffeves, G. Nogues, M. Brune, and S. Haroche, J. Phys. B **38**, S535 (2005).
[3] R. Miller *et al.*, J. Phys. B **38**, S551 (2005).
[4] A. Wallraff *et al.*, Nature (London) **431**, 162 (2004).
[5] L. DiCarlo *et al.*, Nature (London) **460**, 240 (2009).
[6] R. Vijay, D. H. Slichter, and I. Siddiqi, Phys. Rev. Lett. **106**, 110502 (2011).
[7] M. Hatridge *et al.*, Science **339**, 178 (2013).
[8] A. A. Houck *et al.*, Nature (London) **449**, 328 (2007).
[9] C. Eichler, C. Lang, J. M. Fink, J. Govenius, S. Filipp, and A. Wallraff, Phys. Rev. Lett. **109**, 240501 (2012).
[10] P. J. Leek, M. Baur, J. M. Fink, R. Bianchetti, L. Steffen, S. Filipp, and A. Wallraff, Phys. Rev. Lett. **104**, 100504 (2010).
[11] M. Mariantoni *et al.*, Nat. Phys. **7**, 287 (2011).
[12] D. Gottesman, A. Kitaev, and J. Preskill, Phys. Rev. A **64**, 012310 (2001).
[13] Z. Leghtas, G. Kirchmair, B. Vlastakis, R. J. Schoelkopf, M. H. Devoret, and M. Mirrahimi, Phys. Rev. Lett. **111**, 120501 (2013).

[14] M. Hofheinz *et al.*, Nature (London) **454**, 310 (2008).
[15] M. Hofheinz *et al.*, Nature (London) **459**, 546 (2009).
[16] R. Hanson, L. P. Kouwenhoven, J. R. Petta, S. Tarucha, and L. M. L. Vandersypen, Rev. Mod. Phys. **79**, 1217 (2007).
[17] K. D. Petersson, L. W. McFaul, M. D. Schroer, M. Jung, J. M. Taylor, A. A. Houck, and J. R. Petta, Nature (London) **490**, 380 (2012).
[18] M. Trif, V. N. Golovach, and D. Loss, Phys. Rev. B **77**, 045434 (2008).
[19] P. Q. Jin, M. Marthaler, A. Shnirman, and G. Schon, Phys. Rev. Lett. **108**, 190506 (2012).
[20] X. Hu, Y. X. Liu, and F. Nori, Phys. Rev. B **86**, 035314 (2012).
[21] T. Frey, P. J. Leek, M. Beck, A. Blais, T. Ihn, K. Ensslin, and A. Wallraff, Phys. Rev. Lett. **108**, 046807 (2012).
[22] H. Toida, T. Nakajima, and S. Komiyama, Phys. Rev. Lett. **110**, 066802 (2013).
[23] J. J. Viennot, M. C. Dartiailh, A. Cottet, and T. Kontos, Science **349**, 408 (2015).
[24] G.-W. Deng, D. Wei, J. R. Johansson, M.-L. Zhang, S.-X. Li, H.-O. Li, G. Cao, M. Xiao, T. Tu, G.-C. Guo, H.-W. Jiang, F. Nori, and G.-P. Guo, Phys. Rev. Lett. **115**, 126804 (2015).
[25] L. Viola, S. Lloyd, and E. Knill, Phys. Rev. Lett. **83**, 4888 (1999).
[26] G. de Lange, Z. H. Wang, D. Riste, V. V. Dobrovitski, and R. Hanson, Science **330**, 60 (2010).
[27] C. A. Ryan, J. S. Hodges, and D. G. Cory, Phys. Rev. Lett. **105**, 200402 (2010).
[28] C. Barthel, J. Medford, C. M. Marcus, M. P. Hanson, and A. C. Gossard, Phys. Rev. Lett. **105**, 266808 (2010).
[29] H. Bluhm *et al.*, Nat. Phys. **7**, 109 (2011).
[30] J. Bylander *et al.*, Nat. Phys. **7**, 565 (2011).
[31] M. J. Biercuk *et al.*, Nature (London) **458**, 996 (2009).
[32] Y. Sagi, I. Almog, and N. Davidson, Phys. Rev. Lett. **105**, 053201 (2010).
[33] J. Du *et al.*, Nature (London) **461**, 1265 (2009).
[34] J. R. West, D. A. Lidar, B. H. Fong, and M. F. Gyure, Phys. Rev. Lett. **105**, 230503 (2010).
[35] H. K. Ng, D. A. Lidar, and J. Preskill, Phys. Rev. A **84**, 012305 (2011).
[36] T. van der Sar *et al.*, Nature (London) **484**, 82 (2012).
[37] J. R. Petta *et al.*, Science **309**, 2180 (2005).
[38] S. Foletti *et al.*, Nat. Phys. **5**, 903 (2009).
[39] M. D. Shulman *et al.*, Science **336**, 202 (2012).
[40] L. Childress, A. S. Sorensen, and M. D. Lukin, Phys. Rev. A **69**, 042302 (2004).
[41] G. P. Guo, H. Zhang, Y. Hu, T. Tu, and G. C. Guo, Phys. Rev. A **78**, 020302(R) (2008).
[42] Z. R. Lin, G. P. Guo, T. Tu, F. Y. Zhu, and G. C. Guo, Phys. Rev. Lett. **101**, 230501 (2008).
[43] O. E. Dial, M. D. Shulman, S. P. Harvey, H. Bluhm, V. Umansky, and A. Yacoby, Phys. Rev. Lett. **110**, 146804 (2013).
[44] D. J. Reilly, J. M. Taylor, E. A. Laird, J. R. Petta, C. M. Marcus, M. P. Hanson, and A. C. Gossard, Phys. Rev. Lett. **101**, 236803 (2008).
[45] B. Vlastakis *et al.*, Science **342**, 607 (2013).
[46] K. Khodjasteh, D. A. Lidar, and L. Viola, Phys. Rev. Lett. **104**, 090501 (2010).
[47] M. D. Grace, J. M. Dominy, W. M. Witzel, and M. S. Carroll, Phys. Rev. A **85**, 052313 (2012).
[48] X. Wang, L. S. Bishop, J. P. Kestner, E. Barnes, K. Sun, and S. Das Sarma, Nat. Commun. **3**, 997 (2012).
[49] J. P. Kestner, X. Wang, L. S. Bishop, E. Barnes, and S. Das Sarma, Phys. Rev. Lett. **110**, 140502 (2013).
[50] P. Cerfontaine, T. Botzem, D. P. DiVincenzo, and H. Bluhm, Phys. Rev. Lett. **113**, 150501 (2014).
[51] L. Cywinski, W. M. Witzel, and S. Das Sarma, Phys. Rev. Lett. **102**, 057601 (2009).
[52] E. Barnes, L. Cywinski, and S. Das Sarma, Phys. Rev. Lett. **109**, 140403 (2012).
[53] X. Hu and S. Das Sarma, Phys. Rev. Lett. **96**, 100501 (2006).
[54] A. Blais, R. S. Huang, A. Wallraff, S. M. Girvin, and R. J. Schoelkopf, Phys. Rev. A **69**, 062320 (2004).
[55] R. S. Huang, Ph.D. thesis, Indiana University, 2004.
[56] G. Lindblad, Commun. Math. Phys. **48**, 119 (1976).
[57] M. A. Nielsen and I. L. Chuang, *Quantum Computation and Quantum Information* (Cambridge University Press, Cambridge, England, 2000).
[58] H. P. Breuer and F. Petruccione, *Theory of Open Quantum Systems* (Oxford University Press, New York, 2007).
[59] H. Bluhm, S. Foletti, D. Mahalu, V. Umansky, and A. Yacoby, Phys. Rev. Lett. **105**, 216803 (2010).
[60] Y. Dovzhenko, J. Stehlik, K. D. Petersson, J. R. Petta, H. Lu, and A. C. Gossard, Phys. Rev. B **84**, 161302(R) (2011).
[61] Z. Shi, C. B. Simmons, D. R. Ward, J. R. Prance, X. Wu, T. S. Koh, J. K. Gamble, D. E. Savage, M. G. Lagally, M. Friesen, S. N. Coppersmith, and M. A. Eriksson, Nat. Commun. **5**, 3020 (2014).
[62] T. S. Koh, S. N. Coppersmith, and M. Friesen, Proc. Natl. Acad. Sci. USA **110**, 19695 (2013).
[63] A. M. Souza, G. A. Alvarez, and D. Suter, Phys. Rev. Lett. **106**, 240501 (2011).